



Cytochrome c_1 exhibits two binding sites for cytochrome c in plants



Blas Moreno-Beltrán^a, Antonio Díaz-Quintana^a, Katuska González-Arzola^a, Adrián Velázquez-Campoy^{b,c,d}, Miguel A. De la Rosa^a, Irene Díaz-Moreno^{a,*}

^a Instituto de Bioquímica Vegetal y Fotosíntesis, cicCartuja, Universidad de Sevilla - CSIC, Avda. Américo Vespucio 49, Sevilla 41092, Spain

^b Institute of Biocomputation and Physics of Complex Systems (BIFI)-Joint Unit BIFI-IQFR (CSIC), Universidad de Zaragoza, Mariano Esquillor s/n, 50018, Zaragoza, Spain

^c Departamento de Bioquímica y Biología Molecular y Celular, Universidad de Zaragoza, Pedro Cerbuna 12, 50009, Zaragoza, Spain

^d Fundación ARAID, Government of Aragón, María de Luna 11, 50018, Zaragoza, Spain

ARTICLE INFO

Article history:

Received 17 March 2014

Received in revised form 23 July 2014

Accepted 26 July 2014

Available online 1 August 2014

Keywords:

Arabidopsis thaliana

Cytochrome c

Cytochrome bc_1 complex

NMR

Respirasome

Supercomplex

ABSTRACT

In plants, channeling of cytochrome c molecules between complexes III and IV has been purported to shuttle electrons within the supercomplexes instead of carrying electrons by random diffusion across the intermembrane bulk phase. However, the mode plant cytochrome c behaves inside a supercomplex such as the respirasome, formed by complexes I, III and IV, remains obscure from a structural point of view. Here, we report *ab-initio* Brownian dynamics calculations and nuclear magnetic resonance-driven docking computations showing two binding sites for plant cytochrome c at the head soluble domain of plant cytochrome c_1 , namely a non-productive (or *distal*) site with a long heme-to-heme distance and a functional (or *proximal*) site with the two heme groups close enough as to allow electron transfer. As inferred from isothermal titration calorimetry experiments, the two binding sites exhibit different equilibrium dissociation constants, for both reduced and oxidized species, that are all within the micromolar range, thus revealing the transient nature of such a respiratory complex. Although the docking of cytochrome c at the *distal* site occurs at the interface between cytochrome c_1 and the Rieske subunit, it is fully compatible with the complex III structure. In our model, the extra *distal* site in complex III could indeed facilitate the functional cytochrome c channeling towards complex IV by building a “floating boat bridge” of cytochrome c molecules (between complexes III and IV) in plant respirasome.

© 2014 Elsevier B.V. All rights reserved.

1. Introduction

Cytochrome c (Cc) was first described as a redox carrier in the mitochondrial electron transport chain transferring electrons from cytochrome bc_1 (Cbc₁) to cytochrome c oxidase (CcO), which are respectively known as complexes III and IV [1–3]. Since then, several other mitochondrial Cc partners were being reported, including recently the flavoenzyme L-galactono-1,4-lactone dehydrogenase (GALDH) in plants; GALDH is required for the correct assembly of NADH dehydrogenase (or complex I) and catalyzes the terminal step of L-ascorbate biosynthesis [4–6]. Nowadays, Cc is capable of interacting with several protein targets not only in the mitochondria under homeostatic

conditions but also in the cytoplasm and even in the nucleus under programmed cell death conditions [7–10].

Nowadays, the organization and dynamics of the respiratory complexes in the inner mitochondrial membrane are a matter of debate, for which two different models have been proposed [11]. In the random collision models, all membrane proteins and redox components catalyzing electron transport and ATP synthesis are in constant and independent diffusional motion [12]. In contrast, the supramolecular organization models of membranes are based on specific interactions between individual respiratory complexes to form stable supercomplexes. In fact, the oligomerization in supercomplexes could enhance the respiratory chain activity through spatial restriction of electron carrier diffusion [13]. In particular, the complexes I, III and IV are, in their turn, the three basic components of the so-called respirasome, which is a multisubunit respiratory supercomplex composed of dimeric complex III and single copies of complexes I and IV [14]. Such a diversity in arrangement of the respiratory complexes may modulate the capability of cells in response to diverse environmental conditions [15] as the respirasome could quickly drive electrons from NADH to dioxygen in the presence of ubiquinone and Cc [16,17].

In this context, Cc channeling between complexes III and IV to shuttle electrons within the supercomplexes instead of carrying them by random diffusion has recently been proposed to occur in plants [18],

Abbreviations: AIRs, ambiguous interaction restraints; AU, analytical ultracentrifugation; BD, Brownian dynamics; Cc, cytochrome c ; Cc₁, cytochrome c_1 ; Cc₂, cytochrome c_2 ; Cbc₁, cytochrome bc_1 complex; CcO, cytochrome c oxidase complex; Cf, cytochrome f ; CD, circular dichroism; CSP, chemical-shift perturbations; ET, electron transfer; GALDH, L-galactono-1,4-lactone dehydrogenase; HADDOCK, High Ambiguity Driven Docking approach; HSQC, heteronuclear single-quantum correlation; ITC, isothermal titration calorimetry; MD, molecular dynamics; NMR, nuclear magnetic resonance; PCA, principal component analysis; pCc, plant cytochrome c ; pCc_{red}, reduced plant cytochrome c ; pCc_{ox}, oxidized plant cytochrome c ; pCc₁, plant Cytochrome c_1 ; pCc_{1ox}, oxidized plant cytochrome c_1 ; pCc_{1red}, reduced plant cytochrome c_1 ; pRieske, plant Rieske

* Corresponding author. Tel.: +34 954489513; fax: +34 954460165.

E-mail address: idiazmoreno@us.es (I. Díaz-Moreno).

in agreement with the metabolic channeling model proposed by Kholodenko and Westerhoff [19]. Within this frame, channeling would imply the affinity of Cc molecules towards consecutive binding sites, impairing its release to the bulk phase but providing a diffusion path between its redox partners. This idea demands a detailed structural and functional analysis of the interactions between plant Cc (pCc) and its respiratory partners. The structure of the mammalian supercomplexes is consistent with a single Cc molecule bound to one of the Cc₁ subunits of complex III, as found in the yeast X-ray structure [20,21]. Unfortunately, the behavior of pCc in supercomplexes remains obscure from a structural point of view as not even the electron tomography studies of plant respirasomes have revealed the location of pCc molecules [22].

In classical redox experiments, Cc seems to interact with either complex III or IV by forming multiple transient encounters that enable high turnover rates and efficient electron transfer (ET), even though only a few conformations of the encounter ensemble lead to a productive complex [20,23,24]. Actually, the multiphasic kinetics observed in polarographic and spectrophotometric assays for the oxidation of reduced Cc by beef complex IV can be fitted to a model with just one catalytic site. Such a simple model includes alternative binding conformations of the transient complex, with some of them being unable to transfer electrons but affecting the ET rate at the catalytic site [25,26]. Recently, the surface residues of human Cc contacting bovine complex IV have been mapped by nuclear magnetic resonance (NMR) [27].

Non-ET conformations within the complex between beef Cbc₁ and human Cc were also evidenced by steady state kinetic analysis, and so a binding model with more than one molecule of Cc per molecule of Cbc₁ was proposed to explain the observed multiphasic kinetics [28]. In addition, a second cytochrome c₂ (Cc₂) binding site was proposed for the biphasic kinetic observed by plasmon resonance in the oxidized Cbc₁–Cc₂ complex from *Rhodobacter capsulatus* [29]. However, the crystal structure of the yeast Cbc₁–Cc complex does only show a single Cc molecule on the native complex III dimer, mainly driven by non-polar contacts [20,30,31]. Notwithstanding, extra electrostatically charged residues seem to be also involved, as inferred from molecular dynamics (MD) calculations [32] and experimental data with chemically modified Cc [33,34].

The Cbc₁–Cc interaction corresponds to a short-lived complex, whose lifetime and ET mechanism are strongly dependent on ionic strength [35,36]. Ruthenium-based techniques of photooxidation have been developed to study ET in the Cbc₁–Cc complex from *Rhodobacter sphaeroides*, *Paracoccus denitrificans* and yeasts [36–40]. The resulting kinetic data suggest the formation of an encounter complex guided by long-range electrostatic forces. Interestingly, ruthenium kinetics have also shown that the acidic domain of the Cbc₁ complex from *R. sphaeroides*, which is analogous to the acidic subunits in eukaryotic bc₁ complexes, does not play any significant role in ET [40].

The nature of non-productive conformations within the Cbc₁–Cc complex and their eventual role in the respirasome assembly remain unclear. In this work, we have investigated the interaction in solution between pCc and the globular domain of plant cytochrome c₁ (pCc₁), which has been made soluble by truncating its membrane-anchoring hydrophobic helix located at the extreme C terminus (Fig. 1). The transient complex between the two *Arabidopsis thaliana* heme proteins has been here analyzed by using NMR, isothermal titration calorimetry (ITC) and restraint docking calculations. Surprisingly, our experimental data reveal two well-defined binding sites for pCc at the pCc₁ surface, namely a non-productive (or *distal*) site with a long heme-to-heme distance (>30 Å) and a functional (or *proximal*) site with the two heme groups close enough (<8 Å) as to allow ET. Though not functionally active in redox reactions, the *distal* site at the pCc₁ adduct could play a key role in channeling pCc molecules within the respiratory mitochondrial supercomplexes in plants.

2. Material and methods

2.1. Design of constructs and site-directed mutagenesis

A 0.72 kb synthetic DNA fragment encoding for the soluble domain of pCc₁ subunit (amino acids 64–265, GenBank ID: [834081](#)) fused to a standard N-terminal periplasmic signal peptide was amplified by PCR using the oligonucleotides pCc₁_fw (5-GCGGGATCCAGGAGGTGACCA TG-3) and pCc₁_rv (5-GCGCTCGAGTTCATTTCGGTTCGC-3), containing *Bam*HI and *Xho*I restriction sites (underlined), respectively. The reaction product was inserted in the pET28a(+) expression vector. Successful cloning was confirmed by automated sequencing. Site-directed mutagenesis was performed using pET_pCc₁ as a template and the QuikChange II method (Stratagene, <http://www.stratagene.com>). The primers for PCR were pCc₁_C10A_fw (5-TGGCCTGGAAGC GCCGAATAT-3) and pCc₁_C10A_rv (5-ATAGTTCGGCGCTTCACGGC CA-3).

A 0.4 kb DNA fragment encoding for the pCc was cloned into a pBTR1 vector [41] by adaptamer technology. The pBTR1 contains the yeast hemelyase, needed for correct heme integration in c-type cytochromes. The oligonucleotides used to generate the adaptamer were pCc_adapt_fw (5-ATATATCCATGGCGTCATTGA-3) and pCc_adapt_rv (5-TCTTGGTACC TCATCAGCGGT-3). pCc DNA insert was amplified directly from pCytA [42]. The pET_pCc₁-C10A and pBTR-pCc constructs were verified by automated sequencing.

Protein expression and purification protocols have been included in Supplementary Material (Materials and Methods M1).

2.2. Absorption spectroscopy

Absorption spectra were recorded in the ultraviolet–visible (UV–VIS) range at 25 °C in a V-650 spectrophotometer (Jasco, <http://www.jascoinc.com>). A 1 ml quartz cuvette with a path length of 10 mm was employed. Circular dichroism (CD) spectra were recorded in the UV range (190–250 nm) at 25 °C in a J-815 spectropolarimeter (Jasco, <http://www.jascoinc.com>), equipped with a Peltier temperature-control system, using a 1-mm quartz cuvette. Protein concentration was 3 µM in 5 mM sodium phosphate buffer (pH 6.3). Twenty scans were averaged out for each sample. Secondary structure analysis was performed by using CDPPO software [43,44]. CDSSTR was used as reference database.

2.3. Analytical ultracentrifugation

Sedimentation equilibrium experiments of pCc₁ were performed at 20 °C in an Optima XL-A Analytical Ultracentrifuge (Beckman Instruments, <https://www.beckmancoulter.com>) with an AN50-Ti rotor. 80 µL aliquots of a 50 µM pCc₁ solution in 5 mM sodium phosphate buffer (pH 6.3) were analyzed at three successive speeds (13,000; 15,300 and 22,500 rpm). Absorbance was measured at 523 nm after 17 h to ensure that the equilibrium condition was reached. Baseline signals were determined taking a radial scan at 13,000 rpm after running the samples for 8 h at 45,000 rpm. Conservation of mass in the cell was checked in all experiments. Sedimentation velocity experiments were performed at 45,000 rpm and 20 °C with 400 µL samples loaded into double sector cells, using the same buffer and protein concentration as in the equilibrium experiments. Radial scans at 523 nm were taken every 10 min and the sedimentation coefficient distribution was calculated by least-squares boundary modeling of the sedimentation velocity data using the program SEDFIT [45]. The experimental coefficients were converted to standard conditions. The partial specific volume of pCc₁ (0.738 g/L), calculated from the amino acid composition, as well as the buffer density and viscosity were determined with the SEDNTERP program [46].

2.4. NMR measurements

1D ^1H NMR spectra of pCc₁ in its two redox states were performed on a Bruker Avance 700 MHz (Bruker, <http://www.bruker.com>). Water signal was suppressed by WATERGATE solvent suppression method [47]. Protein concentration was 100 μM in 5 mM sodium phosphate buffer (pH 6.3). Either ascorbic acid or ferricyanide was added to ensure the redox state for each sample. NMR assignments of the ^{15}N and ^1H nuclei of reduced pCc (pCc_{red}, BMRB accession number 18828) were taken from previous work [6]. The data were processed using Bruker TOPSPIN (Bruker) and then analyzed with SPARKY (T. D. Goddard and D. G. Kneller, SPARKY 3, University of California, San Francisco, CA, USA).

NMR titrations of 100 μM of ^{15}N labeled pCc with aliquots of unlabeled pCc₁ (both reduced) were performed in 5 mM sodium phosphate (pH 6.3) and 10% D₂O. Each titration step was prepared in an independent NMR tube (Shigemi) up to a 0.28 ml volume. The pH of the samples was checked before and after recording every spectrum. The chemical-shift changes were monitored in a series of [^1H , ^{15}N] Heteronuclear Single-Quantum Correlation (HSQC) experiments at 25 °C and recorded on a Bruker Avance 700 MHz (Bruker). The data were processed using Bruker TOPSPIN (Bruker) and analyzed with SPARKY. NMR chemical-shift titration curves were analyzed with Origin 7 (OriginLab, <http://www.originlab.com>) by using a two-parameter non-linear least squares fit using a one-site (1) and two-site (2) binding model. Under fast exchange conditions, the chemical-shift perturbations (CSP) for a signal in a given titration step is defined by:

$$\Delta\delta = \frac{[A]_b}{[A]_0} \Delta\delta_{\max} \quad (1)$$

where

$$[A]_0 = [A]_f + [A]_b$$

$$[A]_f = \frac{[A]_0 - [B]_0 - K_D - \sqrt{(K_D + [B]_0 - [A]_0)^2 + 4 \cdot K_D \cdot [A]_0}}{2}$$

$$[A]_b = \frac{[A]_0 + [B]_0 + K_D - \sqrt{(K_D + [B]_0 - [A]_0)^2 + 4 \cdot K_D \cdot [A]_0}}{2}$$

wherein $\Delta\delta_{\max}$ is the maximum perturbation for the signal, and $[A]_0$ and $[B]_0$ are the overall and respective concentrations of pCc and pCc₁ in the measured sample. $[A]_f$ and $[A]_b$ are the concentrations of the free and bonded pCc species under equilibrium. K_D is the dissociation constant. The equation deduction is in Supplementary Material (Materials and Methods M2).

For the two-binding sites, the third order equation was solved according to the approach of Wang and Jiang [48]. In this approach, two sites with different affinities are considered, and each one of them can be in different accessibility states. For simplicity, we assumed a full ability of the two sites in pCc₁ to bind pCc. Thus:

$$\Delta\delta = \Delta\delta_{\max} \cdot \frac{\left([A]_0 + \frac{a}{3} - \frac{2}{3}\sqrt{(a^2 - 3b)} \cdot \cos\frac{\theta}{3}\right)}{[A]_0} \quad (2)$$

where

$$\theta = \arccos \frac{-2 \cdot a^3 + 9 \cdot a \cdot b - 27 \cdot c}{2\sqrt{(a^2 - 3 \cdot b)^3}};$$

$$a = K_{D1} + K_{D2} + 2 \cdot [B]_0 - [A]_0;$$

$$b = K_{D1} \times K_{D2} + (K_{D1} + K_{D2}) \cdot ([B]_0 - [A]_0); \text{ and}$$

$$c = -K_{D1} \cdot K_{D2} \cdot [A]_0.$$

The average CSP were derived from the equation:

$$\Delta\delta_{\text{avg}} = \frac{\sqrt{(\Delta\delta^N/5)^2 + (\Delta\delta^H)^2}}{2}$$

where $\Delta\delta^N$ and $\Delta\delta^H$ are the CSP of the amide nitrogen and proton, respectively. The estimated error in K_D values was 10%.

The methods for the global fitting of CSP and determination of line broadenings are in Supplementary Material (Materials and Methods M3 and M4). The principal component analysis (PCA) method is also in Supplementary Material (Materials and Methods M5).

2.5. ITC measurements

All ITC experiments were performed using an Auto-ITC200 instrument (GE Healthcare, <http://www.gehealthcare.com>) at 25 °C. The reference cell was filled with distilled water. The titration experiments between pCc₁ and pCc consisted of 2 μl injections of 0.4 mM pCc (reduced or oxidized forms) in 10 mM sodium phosphate buffer pH 7.4 into the sample cell, initially containing 20 μM pCc₁ solution (reduced or oxidized) exactly in the same buffer. All solutions were degassed before the titrations. The titrant was injected at appropriate time intervals to ensure the thermal power signal returned to the baseline prior to the next injection. To achieve homogeneous mixing in the cell, the stirring speed was kept constant at 1000 rpm. The data, specifically the heat per injection normalized per mol of injectant versus molar ratio, were analyzed with Origin 7 (OriginLab) using a two-site binding model [49]. Calibration and performance tests of the calorimeter were carried out conducting CaCl₂-EDTA titrations with solutions provided by the manufacturer. The values of the reduced χ^2 statistic were calculated considering the normalized heat associated with each injection Q, expressed in calories per mol.

2.6. Brownian dynamics

Brownian dynamics (BD) trajectories were computed for *ab initio* docking with the SDA-6 package [50]. For this purpose, PQR files were built using the LEAP module of AMBER 9 [51] using the AMBER 2003 force-field charge set [52]. Then, a 97 Å³ electrostatic grid with 1 Å node spacing was built with the APBS package [53]. Ionic strength was set to 100 mM and the protein internal dielectric was 4. Translational and rotational diffusion constants for BD were calculated from the initial coordinates using the script ARO (former main_axis) [54] on the tcl console of VMD [55]. Every complex formed was recorded except when the RMSD value was lower than 2 Å with respect to a previous one. A structural alignment of modeled proteins to the X-ray coordinates for the yeast complex [30] was applied as an accuracy reference. Structures were represented using UCSF Chimera [56].

2.7. NMR-driven docking

Restrained docking calculations were performed with the High Ambiguity Driven Docking approach (HADDOCK) [57–59], using homology models as input for reduced forms of pCc, pCc₁ and plant Rieske head domain (pRieske) (Supplementary Material, Materials and Methods M6). Dielectric constant was set distance-dependent. Scaling of intermolecular interactions for rigid body was fixed to 1.0. Ambiguous interaction restraints (AIRs) for the docking simulation were generated using standard criteria. Random exclusion of AIRs was not employed. pCc residues labeled as active were those showing $\Delta\delta_{\text{avg}} \geq 0.025$ ppm and a solvent accessibility larger than 50%, calculated with NACCESS.

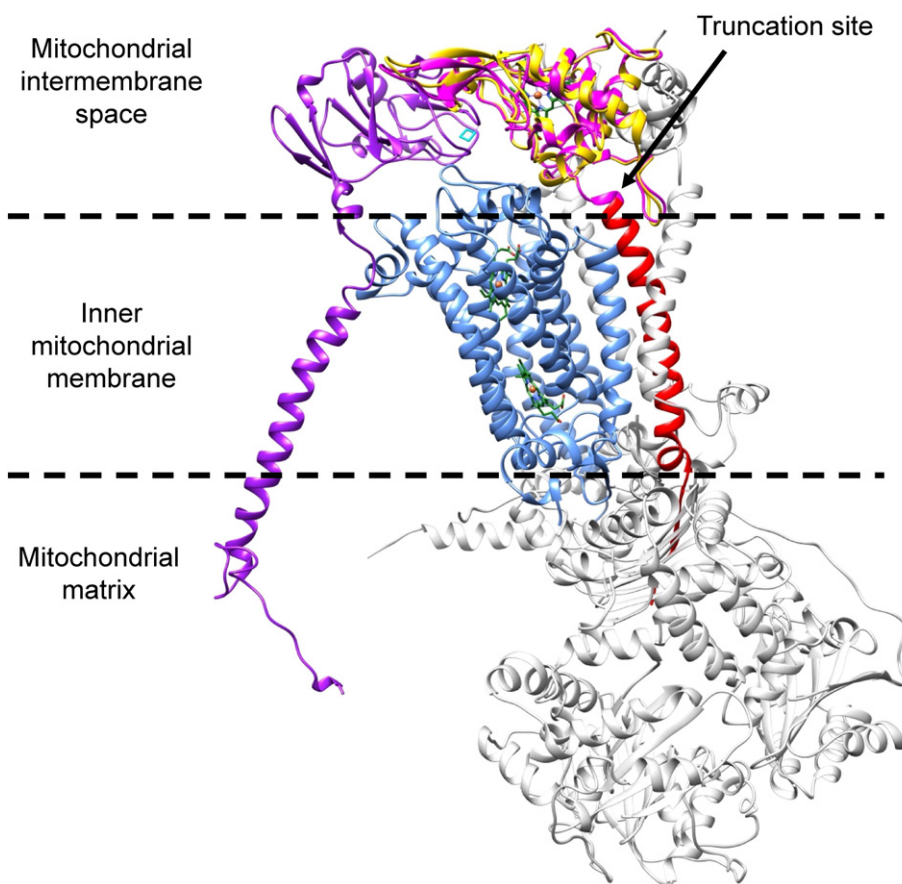


Fig. 1. The functional *Cbc1* monomer. Chimeric model of complex III based on the structure of the functional monomer from yeast *Cbc1* (PDB: 1kyo) with its cytochrome *b* subunit colored in blue. The Rieske subunit, shown in purple, has been replaced by the chicken Rieske subunit (PDB: 1bcc) at its “open” conformation with respect to the quinol oxidation site. The homology model of pCc₁ (in yellow) is overlaid onto the globular domain of yeast Cc₁ subunit (magenta), which has a membrane-anchoring hydrophobic helix that is represented in red. The truncation site of pCc₁ is marked by an arrow. Other yeast complex III subunits are colored in light gray. Heme groups are in green and the iron-sulfur cluster is in cyan.

These active residues were Ala13, Glu15, Lys16, Arg19, Thr20, Gln24, Gln36, Ser55, Ala58, Lys80, Lys81, Gly85, Val89, Lys94 and Lys95. N-terminal residues were not included in the list. pCc residues located at less than 4 Å from the active ones and showing high solvent accessible surface (>50%) were labeled as passive residues. No active residues for pCc₁ were defined and passive residues were those with a high solvent accessibility (>50%). These residues were Gln38, Ser42, Leu48, Arg52, Gly56, Thr60, Glu62, Ala66, Glu70, Val74, Pro77, Asp79, Glu80, Gly81, Glu82, Met83, Thr85, Lys89, Ser91, Arg93, Glu96, Ser99, Glu101, Ser102, Arg105, Phe106, Gly109, Ala122, His124, Arg138, Asp139, Ala142, Gly143, Ser145, Arg147, Glu148, Gly149, Pro157, Asn168, Asp169, Glu170, Glu173, Glu175, Asp176, Gly177, Pro179 and Thr181. Both N- and C-terminal residues were not included in the list. The flexible segments were defined by the active and passive residues used in the AIRs ± 2 sequential amino-acids. For each run, 2000 rigid-body solutions were generated by energy minimization. The 200 structures with lowest AIRs energies were subjected to semi-flexible simulated annealing. Then, the first 100 structures were submitted to a final refinement in explicit water. The 100 best structures were analyzed using standard criteria. Structures were represented using UCSF Chimera [56].

Centers of mass were calculated using previously reported protocol [54]. Second-molecule docking computations were performed with solutions from first pCc₁–pCc molecule docking as input file and a second pCc molecule as probe. Docking parameters and active and passive residues of pCc were defined as before. No active residues for the pCc₁–pCc adduct were defined and passive residues corresponded to those with a high solvent accessibility (>50%). These residues matched with those previously defined for pCc and pCc₁, with the exception of residues from pCc₁ which are not exposed to solvent in pCc₁–pCc adduct. Finally,

single docking computations between the pCc₁–pRieske adduct and pCc were also performed. Only passive residues with high solvent accessibility (>50%) for pCc₁–pRieske were defined. The pCc₁–pRieske complex was built using pCc₁ and pRieske conformations that both structures keep in the “closed” conformation inside complex III [60].

3. Results

3.1. Elucidating two binding sites for pCc on pCc₁

To first understand the nature of the interaction between pCc₁ and pCc and to visualize their ensemble of transient encounter complexes under equilibrium conditions, we computed 2000 BD trajectories with the two heme proteins. Each trajectory lasted 313 ns on average. Fig. 2a shows the distribution of the first, lowest-energy 500 solutions. Notably, pCc swept most of the solvent-exposed pCc₁ surface. For all orientations, non-polar interactions seem to be the largest contribution to binding energy (Table S1), as proposed by Lange and Hunte [30]. The recorded complexes were submitted to structural clustering, which yielded two major clumps. Cluster 1 of Cc molecules comprised 212 recorded structures out of 484,511 matching ones along the trajectories, with the representative Cc structure lying on the same Cc₁ surface patch as in the crystal structure of the yeast *Cbc1*–Cc complex (PDB 1kyo). However, such a representative Cc molecule is rotated by ca. 90°, around the normal to the interaction Cc₁ surface, with respect to Cc orientation in the crystal structure (Fig. 2b and c). As the heme-to-heme distance is short enough to guarantee an efficient ET, this cluster was allocated within the herein called *proximal* binding site. Cluster 2 of Cc molecules consisted of 200 recorded structures out of 361,331

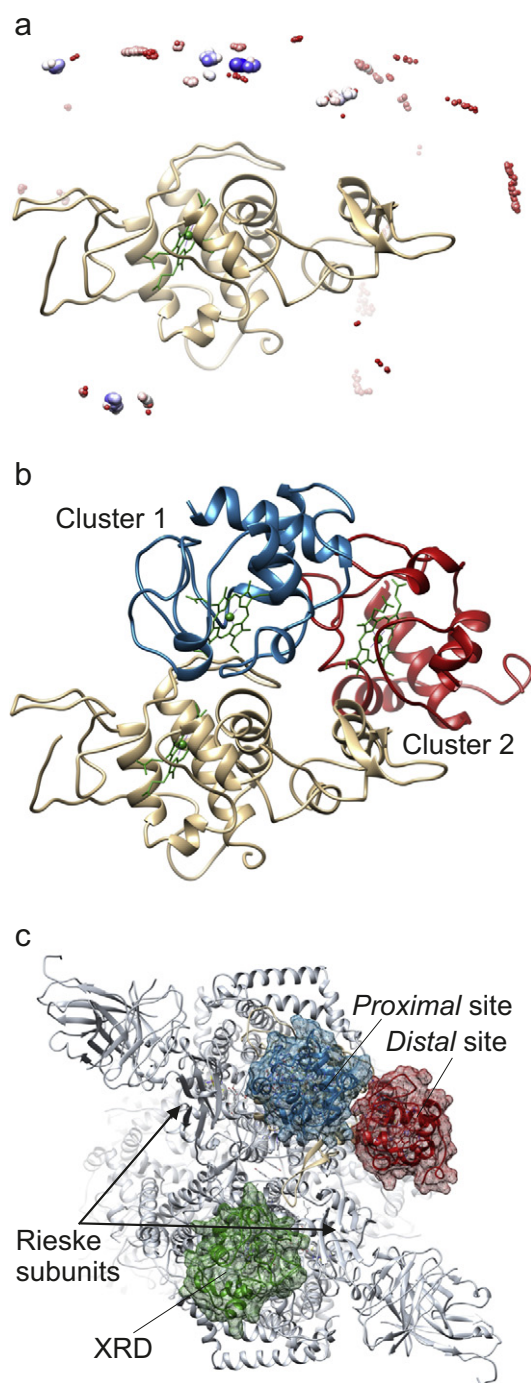


Fig. 2. *Ab-initio* docking calculations of the pCc₁–pCc complex. **a)** Distribution of the mass center of pCc around pCc₁ within the 500 lowest energy conformations of the complex. Every mass center of pCc is represented by a ball colored according to the complex binding energy ranging from $-72 \text{ kcal mol}^{-1}$ (red) to $-92 \text{ kcal mol}^{-1}$ (blue). pCc₁ is represented by a khaki ribbon and the heme group is in green. Orientation of the pCc₁ molecule is the same as in Fig. 1. **b)** Ribbon diagrams showing pCc₁ (khaki) along with the representative Cc structures for clusters 1 (blue) and 2 (red) corresponding to the proximal and distal binding sites of pCc₁, respectively. **c)** View of dimeric complex III from the intermembrane space showing the location of the single Cc molecule in the solved X-ray structure of the yeast Cc-bound complex III (PDB ID: 1kyo, green) in one monomer, and those of the representative Cc structures for proximal (blue) and distal (red) sites in the other monomer, in which the soluble domain of yeast Cc₁ has been replaced by pCc₁, shown in khaki. XRD stands for X-ray diffraction.

matching, and showed ca. 60 Å RMSD from the X-ray structure (Fig. 2b). Remarkably, it sampled at the outer rim of Cc₁ at the Cbc₁ complex (Fig. 2c), and so the adducts were non-ET conformations located at

the herein called *distal* binding site. The remaining clusters were much less populated and, opposite to clusters 1 and 2, they clashed if superposed onto the full Cbc₁ structure.

To test experimentally the stoichiometry of the interaction between pCc₁ and pCc, we cloned the water-soluble and monomeric domain of pCc₁, which keeps its tridimensional structure as compared to the full-length pCc₁ subunit of the Cbc₁ complex in the native membrane. For this purpose, all the residues from the physiological mature protein (GenBank ID: 834081) until Glu265 were kept and the C-terminal hydrophobic helix was removed. The protein sequence of such soluble domain is highly conserved in evolved plants ($\geq 93\%$ sequence identity with rice, soybean, maize, grape vine, tomato, cacao or poplar), whereas the designated position for truncation was selected according to previous works with soluble domains of Cc₁ [24,61–63] and photosynthetic cytochrome *f* (Cf) [64,65]. In addition, Cys10 at the N-terminal region was replaced by alanine to avoid pCc₁ dimerization of wild-type protein through intermolecular disulfide bridges (Fig. S1). The resulting soluble site-directed mutated domain of pCc₁ was expressed in *Escherichia coli*, and analytical ultracentrifugation (AU) corroborated its monomeric state for at least 96% of population (Fig. 3a). The molecular mass of the monomeric domain was 23,857 Da, as verified by MALDI-TOF. Small populations (4%) of multimers were also detected by AU, with a molecular mass of ca. 100.7 kDa.

The proper folding of pCc₁ was assessed by CD and NMR spectroscopies. The CD spectral analysis of reduced pCc₁ (pCc_{1red}) yielded a major α -helix component (67.6%), along with a minor contribution of turns (7.7%) and β -sheets (5%) in the secondary structure (Fig. 3b). Similar results were found for the oxidized state (65.8% of α -helices, 8.6% of turns and 4.3% of β -sheets; Fig. 3b). The 1D ^1H NMR spectrum of pCc_{1red} displayed a high dispersion of signals in the amide and methyl regions, as corresponds to a three-dimensional folding (Fig. 3c, upper). The NMR spectrum also showed several signals at negative δ values that belong to the side chain of Met163 axial ligand, consistent with a proper heme coordination. The 1D ^1H NMR spectrum of oxidized pCc₁ (pCc_{1ox}) showed a significant overall line broadening, and some signals from residues close to the heme group, such as Met163, were strongly shifted as a result of the paramagnetic effect of Fe^{3+} (Fig. 3c, lower).

The UV–VIS absorption spectrum of ascorbate-reduced pCc₁ showed a maximum at 552 (α-band) and at 522 nm (β-band), as expected for the correct incorporation of the heme group into the apoprotein [61, 66]. On the other hand, the oxidized pCc₁ showed the 699-nm band typical of the octahedral heme iron coordination and, in particular, of the bond between the Fe atom and the S δ atom of Met163 (Fig. S2). The calculated redox potential (E_m) of pCc₁ was ca. +160 mV (Fig. S3), lower than that determined (ca. +250 mV) for the membrane-anchored Cc₁ subunit in photosynthetic bacterial and plant complexes [66–68]. Similar decrease in redox potential has also been observed with isolated water-soluble domains of Cc₁ from *R. sphaeroides*, *P. denitrificans* and *Thermus thermophilus* [24,62,63].

The interaction between pCc₁ and pCc was first tested along a direct NMR titration by monitoring the line broadening of the signals from methionine axial ligands of both cytochromes (Met88 of pCc and Met163 of pCc₁, respectively) in their reduced state. As shown in Fig. 4a, the Met88- ϵCH_3 signal of pCc broadened upon every pCc₁ addition. Moreover, the Met163- ϵCH_3 signal of pCc₁ could also be followed at each titration step. This latter also widened with respect to that of unbound pCc₁ at the same concentration level (Fig. 4a).

A CSP analysis of the amide groups of pCc was further performed. For this purpose, NMR titration experiments showing the changes in the $[\text{H}, ^{15}\text{N}]$ HSQC spectrum of ^{15}N -labeled pCc upon gradual addition of pCc₁ were recorded. Several pCc amide signals showed significant chemical-shift displacements along titrations (Fig. 4b), as well as specific line-broadening (Fig. S4), which is consistent with an intermediate/fast exchange rate and with the transient nature of this complex [35,40].

In agreement with BD computations, the CSP binding curves of the titration with reduced proteins could be consistently fitted to a 2:1

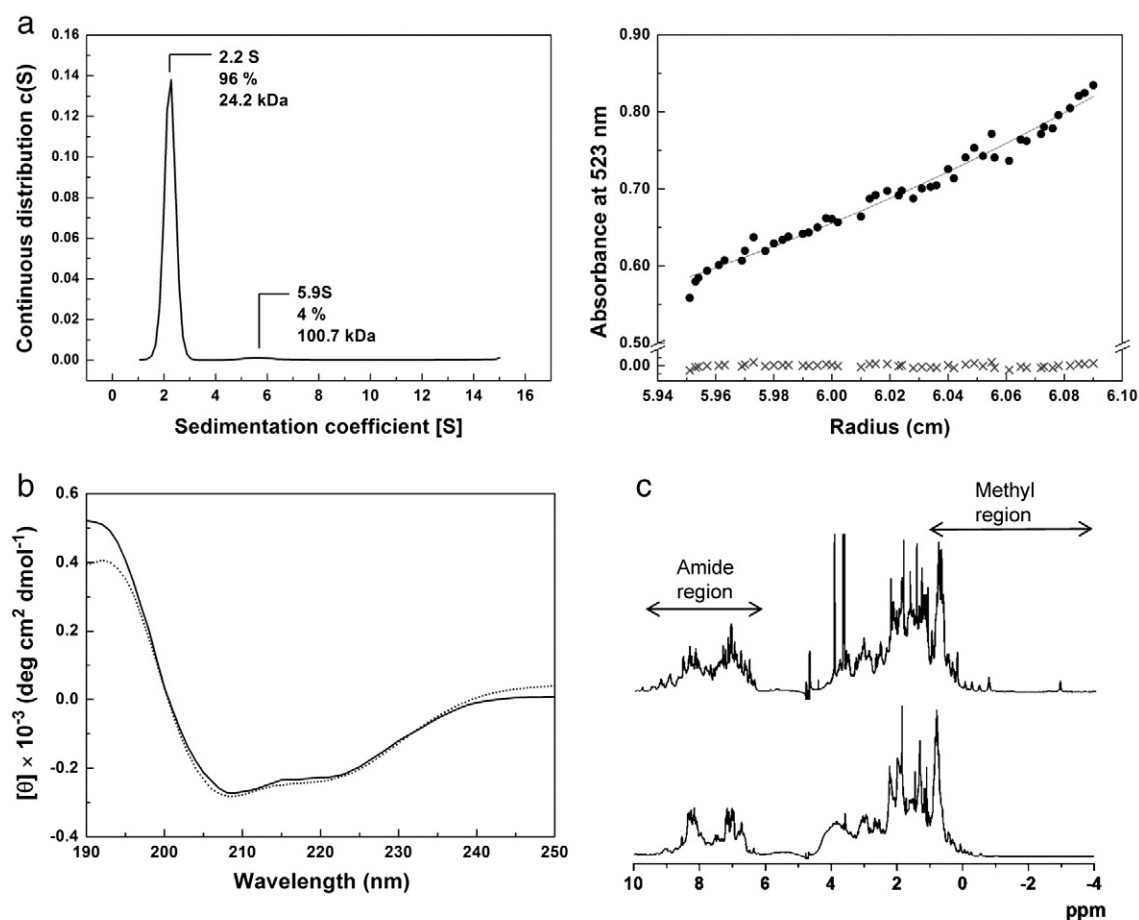


Fig. 3. Biophysical characterization of recombinant pCc₁. **a)** Continuous distribution $c(s)$ versus sedimentation coefficient (left) and sedimentation velocity analysis (right) of reduced pCc₁. **b)** UV CD spectra of reduced (dotted line) and oxidized (solid line) forms of pCc₁. **c)** 1D ^1H NMR spectra of reduced (upper) and oxidized (lower) pCc₁ species.

binding model (two independent binding sites for pCc on pCc₁; Figs. 4c and S5) with all the analyzed amides, according to R^2 and χ^2 statistical criteria. R^2 and χ^2 values were equal to 0.9997 and $2 \cdot 10^{-6}$, respectively. Notably, the binding curves poorly fitted a 1:1 binding model ($R^2 = 0.8183$ and $\chi^2 = 0.0816$), as shown for Gln24 in indirect dimension (Fig. 4d). Hence, the experimental data clearly indicated the presence of two independent pCc binding sites on the pCc₁ surface. The fit to the model described in Material and Methods yielded two different values for the dissociation constant (K_D), namely 0.25 μM for K_{D1} and 30.0 μM for K_{D2} , thereby suggesting a site for tight binding and another site for a weak, more transient interaction (Table 1). The K_{D2} value for the weak-binding site is similar to those reported in other c-type cytochrome ET complexes [65,69–71]. When the two sites were forced to behave with a similar K_D value, the fitting was slightly worse and yielded a K_D value of ca. 9.9 μM , also consistent with a transient complex. In this case, R^2 and χ^2 values were equal to 0.9928 and $3.22 \cdot 10^{-3}$, respectively (Fig. S6).

To further validate the 2:1 binding model, we performed a principal component analysis (PCA) of CSP data. Notably, the first component projection was consistent with ca. 99% of the amplitude of the CSP data and was accurately fitted to a 2:1 stoichiometry with two different K_D values (Fig. S7). Indeed, the binding was fitted to a K_{D1} of 0.29 μM and a K_{D2} of 23 μM . R^2 and χ^2 values were 0.99827 and 0.00576, respectively. These results were in agreement with the previous performed fittings. The fit to one binding site was, by contrast, not good enough. R^2 and χ^2 values were 0.88808 and 0.46825, respectively. The other component projections corresponding to the 1% of the remaining amplitude were not analyzable.

All the pCc signals showed a similar perturbation profile along the NMR titration experiments, a finding suggesting that pCc may use the same surface area to interact with pCc₁ at the two binding sites. The CSP profile and map for the reduced complex (Fig. 4e and f) showed a few residues with $\Delta\delta_{\text{avg}}$ larger than 0.075 ppm. These residues were Phe3, Lys16, Gln24, Lys80, Gly85 and Val89. The map comprised residues at the rim of the heme cleft, such as Thr20, Lys21, Ala23, Gln24, Gln36, Lys87, Val89 and Phe90. The resulting interaction patch is well conserved among complexes involving c-type cytochromes, which include cytochrome c peroxidase, Cf, cytochrome b₅, photosystem I, complex IV, GALDH and novel partners recently discovered [6,10,27,65, 70–75]. In addition, the initial turn of the first α -helix and its interface with the C-terminal helix could likewise be affected by pCc binding to pCc₁.

The CSP map of pCc in Fig. 4f is also consistent with the solved X-ray structure of the yeast Cbc₁–Cc complex (Fig. 4g) [30]. Extensive studies using chemical modification of mammalian Cc have implicated a subset of lysines in the affinity and turnover of Cc in its binding to complex III. Actually, these experiments evidenced the key role of lysines at positions 8, 13, 27, 72, 86 and 87 (residue numbering for mammalian Cc) in the complex III–Cc interaction [33,34], as MD simulations also did [32]. In our solution NMR studies, we have detected significant CSP for the lysines at positions 16, 21, 70, 80, 81, 87, 94 and 95 (residue numbering for pCc). All lysines previously implicated in its binding to complex III were detected, with the only exception of Lys35 (Lys27 in mammalian Cc) that showed a $\Delta\delta_{\text{avg}}$ value lower than 0.025 ppm.

To obtain accurate data on the binding affinities, not only in the reduced system but also in the oxidized complexes, we resorted to ITC

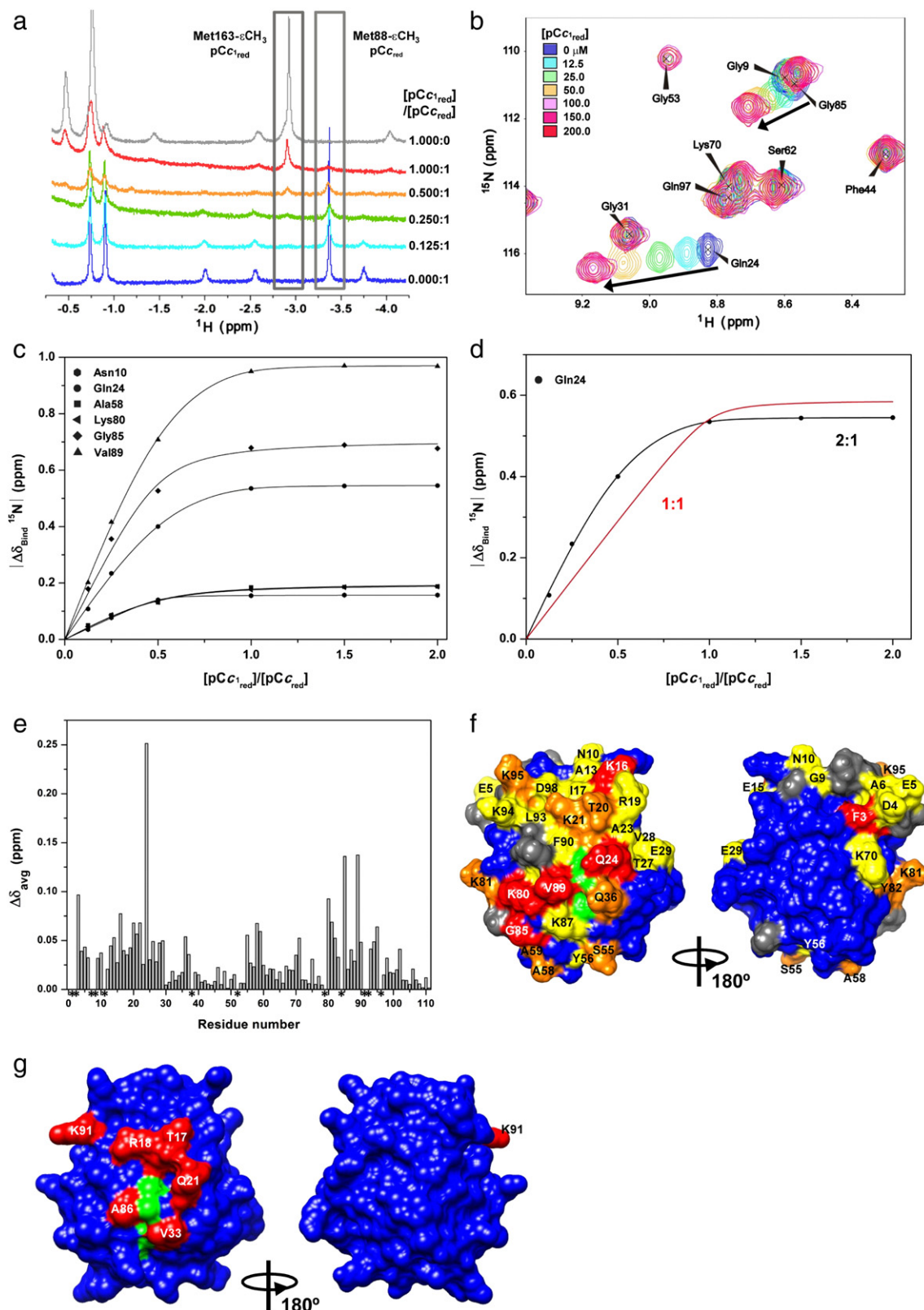


Fig. 4. NMR binding assays of reduced pCc₁-pCc complex. **a**) 1D ^1H NMR spectra of 100 μM pCc₁ along titration with pCc₁. Complex formation can be followed by monitoring the line broadenings of the two heme axial ligand signals (Met163- $\epsilon\text{-CH}_3$ of pCc₁ and Met88- $\epsilon\text{-CH}_3$ of pCc). A control spectrum of 100 μM free pCc₁ is also shown in gray. **b**) Detail of the superimposed $[\text{pCc}_1, ^{15}\text{N}]$ HSQC spectra of ^{15}N -labeled pCc along titration with pCc₁. pCc concentration was 100 μM at each titration step. Signals corresponding to distinct titration steps are colored according to the code in the panel. pCc₁ concentrations at each titration step were depicted in the panel. **c**) Curves representing the best global fit of several amide signals in indirect dimension to a 2:1 ratio for the pCc₁:pCc binding model with two different global K_D values (0.25 for K_{D1} and 30.0 μM for K_{D2}). K_{D1} and K_{D2} stand for the dissociation equilibrium constants of the proximal and distal sites of pCc₁, respectively. **d**) Binding curves of Gln24 in the indirect dimension. Lines represent the best fit to 1:1 (red) or 2:1 (black) binding models. **e**) Plot of CSP of ^{15}N -labeled pCc as a function of residue number. Proline and non-assigned residues are marked by asterisks. **f**) CSP map of reduced pCc upon addition of reduced pCc₁. Residues are colored according to their respective $\Delta\delta_{\text{avg}}$ value, as follows: blue for <0.025 , yellow for ≤ 0.050 , orange for ≤ 0.075 and red for ≤ 0.300 ppm. Prolines and non-assigned are in dark gray, and the heme group is in green. **g**) Surface map of yeast Cc showing in red those residues that are closer than 4 Å to the Cc₁ subunit in the crystal structure of the yeast Cc-bound complex III (PDB ID: 1kyo).

Table 1

Equilibrium and thermodynamic parameters for the interaction of pCc with pCc₁ at the two binding sites. Equilibrium dissociation constants (K_{D1} and K_{D2}), enthalpies (ΔH_1 and ΔH_2), entropies ($-T\Delta S_1$ and $-T\Delta S_2$), Gibbs free energies (ΔG_1 and ΔG_2) and stoichiometry of the reactions (n) were determined by CSP or ITC for the reduced (pCc_{1red}-pCc_{red}) and oxidized (pCc_{1ox}-pCc_{ox}) states.

Protein couple	Proximal site				Distal site				<i>n</i>
	K_{D1} (μM)	ΔH_1 (kcal mol^{-1})	$-T\Delta S_1$ (kcal mol^{-1})	ΔG_1 (kcal mol^{-1})	K_{D2} (μM)	ΔH_2 (kcal mol^{-1})	$-T\Delta S_2$ (kcal mol^{-1})	ΔG_2 (kcal mol^{-1})	
pCc _{1red} /pCc _{red} ^a	0.25	n.d.	n.d.	-8.9	30.0	n.d.	n.d.	-6.1	2
pCc _{1red} /pCc _{red} ^b	6.7	4.3	-11.3	-7.0	35.0	2.4	-8.4	-6.0	2
pCc _{1ox} /pCc _{ox}	9.3	3.0	-9.8	-6.8	110.0	12.0	-17.3	-5.3	2

n.d., not determined.

Relative errors: K_D 20%, ΔH and $-T\Delta S$ 5%, ΔG 2%.

^a CSP.

^b ITC.

experiments (Fig. 5). The experimental data for both redox states fit to a 2:1 model, with two independent binding sites for pCc on pCc₁. The reduced χ^2 value was equal to 504 and 243 for the reduced and oxidized complexes, respectively. As shown in Fig. 5 and Table 1, a first site for tight binding and another site for weak, more transient binding were observed for both redox states. The redox state of the heme proteins slightly affected their binding affinity using both binding sites. Indeed, the reduced system ($K_{D1} = 6.7 \mu\text{M}$, $K_{D2} = 35 \mu\text{M}$) was somewhat tighter than the oxidized system ($K_{D1} = 9.3 \mu\text{M}$, $K_{D2} = 110 \mu\text{M}$). The binding reaction was endothermic for all binding events, in both reduced and oxidized complexes, and was entropically driven. When the two sites were forced to have the same value for K_D , the fitting was less accurate. Indeed, the reduced χ^2 value significantly increased to 2264 and 591 for the reduced and oxidized systems, respectively. In this case, the K_D values were $6.1 \mu\text{M}$ and $22 \mu\text{M}$ for the reduced and oxidized proteins, which is consistent with a lower affinity for the oxidized complex. In

agreement with NMR measurements, the fitting of ITC data to a 1:1 model was slightly worse, as visually shown in Fig. S8.

3.2. Exploring the pCc₁-pCc complex: An NMR-restrained docking model

With our experimental CSP constraints, NMR-restraint docking calculations of the reduced pCc₁-pCc complex were carried out by using the HADDOCK software. Clustering of solutions for NMR-restrained docking resulted in two binding sites on the surface of pCc₁, according to the two-site model suggested by NMR and ITC fitting. In agreement with the BD simulations, non-polar interactions also constituted the major contribution to binding energy; the resulting surface area burials were larger than 1200 \AA^2 (Table 2), whereas those calculated from X-ray coordinates were ca. 990 \AA^2 [20,30,31]. Electrostatic interactions seemed to also be crucial for binding in solution, in consonance with the MD simulations performed by Kokhan et al. [32].

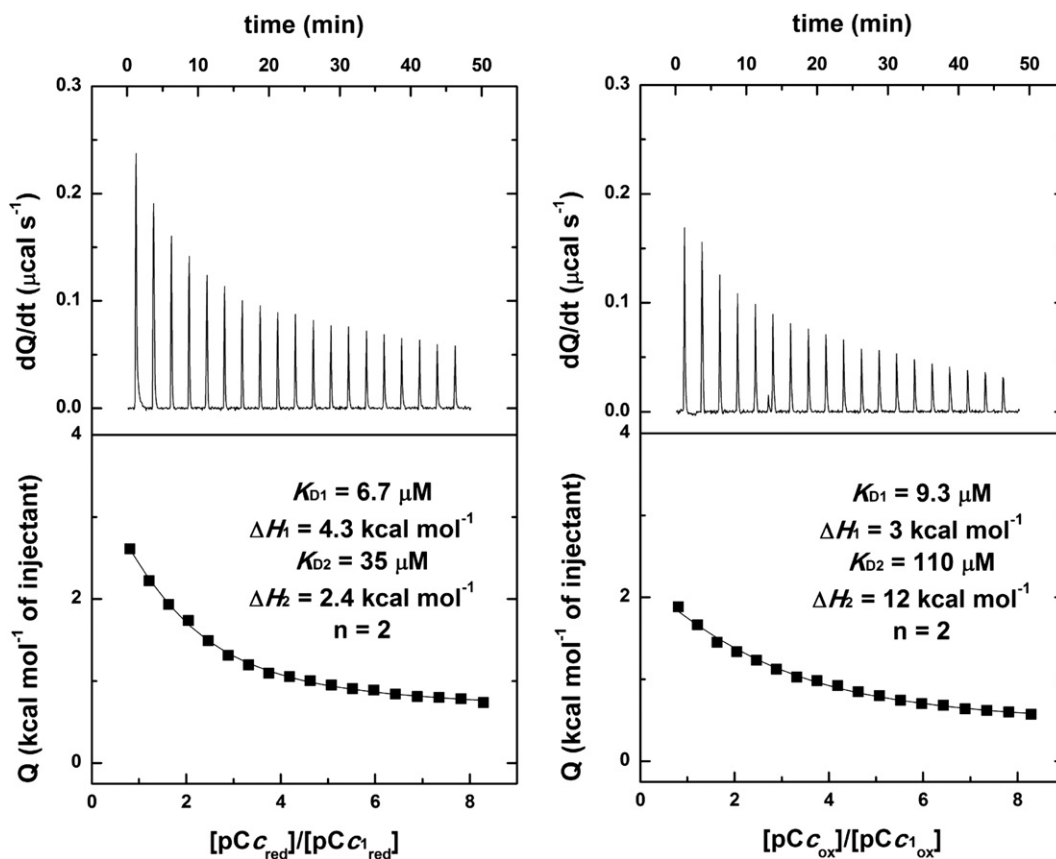


Fig. 5. ITC binding assays of the reduced and oxidized pCc₁-pCc complexes. Binding assays of the complexes between pCc and pCc₁ under reducing (left) or oxidizing conditions (right). The experimental data for both redox states are fitted to a 2:1 model. Thermograms are shown at the upper panels and binding isotherms at the lower panels. pCc₁ concentration in the cell was $20 \mu\text{M}$, whereas pCc concentration in the syringe was $400 \mu\text{M}$.

A first docking between pCc and pCc₁ yielded two clusters of pCc molecules that were compatible with the presence of two independent binding sites for pCc on pCc₁ (Fig. 6a). One of the pCc clusters (cluster 1) coincided with that resulting from the X-ray coordinates of the yeast Cc₁–Cc complex [30] but rotated ca. 90°. Cluster 1 is herein called *proximal* binding site, in which the heme-to-heme distance is ca. 6.7 Å. This site would correspond to the tightest binding site as it matches the crystallographic center of mass of yeast Cc and is consistent with an efficient ET. The second cluster (cluster 2) was located at the outer rim of pCc₁, close to the extended β-strand fork that directly contacts to the Rieske head in complex III. Cluster 2 is herein called *distal* binding site as the two hemes were located far away from each other, at a distance (ca. 36.9 Å) too long for efficient ET. This second site, which is first reported here, would allow a weak binding of pCc to pCc₁. In contrast to cluster 1, the structures from cluster 2 slightly clashed when they were superposed onto the native complex III structure. The two clumps were similarly driven by non-polar and electrostatic interactions, yet the structures in cluster 1 were energetically favored. The backbone deviation was 1.88 Å with respect to the representative structure in each cluster. Although cluster 1 was slightly less populated than cluster 2, it fitted better with the experimental results based on HADDOCK score (Table 2).

To test the independent nature of the purported *distal* site, another single-docking calculation was carried out with the best structure in which pCc sampled the *proximal* site as a starting adduct structure. Two clumps emerging from these computations located nearby to the same surface path of the proposed *distal* site (Fig. 6b) supporting the independence of a second binding governed by non-polar and electrostatic forces (Table 2). Both sub-clusters (2" and 2#) showed similar energy terms and had long heme-to-heme distances (longer than 35 Å), although cluster 2" is clearly more populated. The long distance between redox centers is again consistent with non-ET binding. Notably, the representative structure of cluster 2" did not clash with any subunit when it was superposed on the full dimeric complex III structure.

In addition, a reverse docking calculation was performed to check that the *proximal* binding site was filled when a pCc molecule was fixed on the *distal* binding site of pCc₁ in the starting structure (Fig. S9).

To further assess the reliability and physiological compatibility of the *proximal* and *distal* binding sites, additional docking calculations were carried out. An adduct of pCc₁ bound to pRieske from the same structural monomer was used as starting input. The pRieske subunit was kept in the "open" conformation, with respect to the quinol oxidation site, in the pCc₁–pRieske adduct. Such conformation is more restrictive than the "closed" conformation for pCc sampling on pCc₁ surface [60]. Two clusters were formed on the pCc₁–pRieske surface, which were consistent with our two-site binding model (Fig. 6c and Table 2). Cluster 1* included pCc molecules sampling the *proximal* binding site, which is compatible with ET, and cluster 2* was significantly more populated than cluster 1*. Cluster 2* corresponded to the weak *distal* site located near the interface between pCc₁ and pRieske domain, and did not clash when it was superposed onto the full complex III structure. The

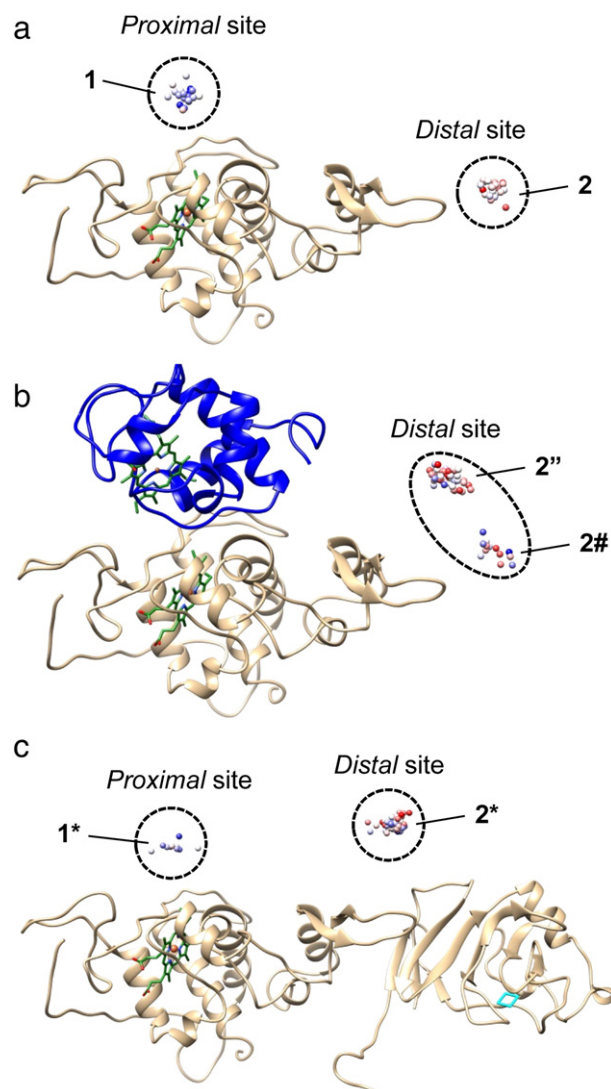


Fig. 6. HADDOCK molecular docking of reduced pCc₁–pCc complex. **a)** Mass centers of pCc were organized in two clusters (1 and 2) that determine two well-defined binding sites in pCc₁, the herein called *proximal* and *distal* sites respectively. Each pCc molecule is plotted as a ball colored according to their intermolecular energy (E_{inter}), ranging from 0 kcal mol^{−1} (red) to −400 kcal mol^{−1} (blue). **b)** Mass centers of pCc from a docking approach in which a pCc molecule was primarily fixed on the *proximal* site. Solutions were colored as a function of E_{inter} , ranging from −50 kcal mol^{−1} (red) to −350 kcal mol^{−1} (blue). pCc molecules at the *distal* binding site were organized in two clusters 2" and 2#. **c)** Additional docking computation using the pCc₁–pRieske adduct. Mass centers of pCc were plotted on the adduct according to its E_{inter} , ranging from −50 kcal mol^{−1} (red) to −450 kcal mol^{−1} (blue). Solutions were divided in two clusters (1* and 2*) as described in a).

intermolecular energy and HADDOCK score ratio between both clusters was not altered by the pRieske subunit. Thus, the existence of a *distal* binding site was fully compatible with the complex III structure.

Table 2
Statistical analysis of HADDOCK data after clustering the solutions for the reduced pCc₁–pCc complex.

Cluster	RMSD (Å)	Size	E_{inter} (kcal mol ^{−1})	$E_{\text{hydrophob}}$ (kcal mol ^{−1})	E_{elec} (kcal mol ^{−1})	Buried surface area (Å ²)	Haddock score (a.u.)
1	1.88 ± 0.57	20	−284 ± 67	−439 ± 55	−387 ± 54	1939 ± 192	−137.7 ± 20
2	1.88 ± 0.52	24	−170 ± 63	−469 ± 49	−449 ± 48	1291 ± 101	−97.8 ± 17
2"	3.38 ± 1.20	39	−76 ± 69	−421 ± 67	−384 ± 89	1472 ± 159	−103.3 ± 15
2#	2.26 ± 0.93	19	−101 ± 55	−429 ± 50	−392 ± 54	1530 ± 118	−103.6 ± 9
1*	1.44 ± 0.62	10	−314 ± 45	−466 ± 46	−421 ± 52	1910 ± 113	−139.1 ± 14
2*	1.48 ± 0.51	56	−222 ± 80	−475 ± 63	−452 ± 05	1833 ± 128	−112.4 ± 12

E_{inter} , $E_{\text{hydrophob}}$ and E_{elec} stand for intermolecular, hydrophobic and electrostatic energy terms.
a.u. stands for arbitrary units.

4. Discussion

It is widely accepted that Cc plays a key role in eukaryotic living cells, under homeostatic conditions, by transferring electrons between the mitochondrial membrane complexes III and IV, either free or associated in supercomplexes [4,14]. However, the way Cc does it within a supercomplex such as the respirasome formed by complexes I, III and IV varies from one organism to another. Actually, pCc seems to be channeled while transferring electrons from complex III to complex IV in plants, but not in mammals [18]. Here, the interaction between pCc and the soluble domain of pCc₁ has been in deep analyzed by combining different experimental approaches.

The physiological significance of the functional analysis herein performed with the soluble domain of pCc₁ is solidly supported by other experimental approaches. In bacteria, for instance, no significant differences are observed in the rate of electron transfer to the soluble acceptor from the Ccb₁ complex, either in its native state or devoid of its soluble acidic domain [40]. Similar approaches have extensively been carried out to analyze the interaction of the photosynthetic electron carriers plastocyanin and cytochrome c₆ with the soluble domain of Cf from the cytochrome b₆f complex [54,64,65,69,71,75].

Our values for the dissociation equilibrium constants of the pCc₁–pCc complex obtained by ITC and NMR are within the micromolar range, so revealing the transient nature of such a respiratory complex in plants. The intermediate/fast exchange regime observed by NMR is consistent with a short-lived complex with lifetimes in the range of μ s–ms [35,40], in which the balance between specificity and turnover is critical for efficient ET. Thus the common association of fast exchange to very weak complexes does not exclude other scenarios. In fact, interprotein complexes under fast exchange with K_D values lower than 0.25 μ M have been reported in literature [76].

In addition, pCc displays a conserved profile of NMR signals in the presence of pCc₁ that mostly belong to residues around the heme crevice. This pattern of pCc signals perturbed upon binding is practically the same when Cc interacts with other physiological targets, such as GALDH, complex IV and novel targets recently discovered [6,10,27]. Our CSP profile is not only compatible with the X-ray structure of yeast Cc bound to yeast complex III [20,30,31], but also reveals extra residues of pCc involved in the binding to pCc₁ in solution.

In the past, the binding interaction between Cc and Cc₁ was often thought to be dominated by electrostatic forces, as inferred from chemical labeling and mutagenesis studies. Actually, well-conserved negatively and positively charged residues around the heme clefts in both cytochromes were identified [33,34]. Our findings here indicate a relevant role of charged residues in solution experiments and docking analyses, pointing out to an electrostatically-driven interaction. These findings are in agreement with the MD simulations performed with the yeast complex III–Cc system and with several ET studies performed in the Cbc₁–Cc complex from *R. sphaeroides*, *P. denitrificans* and yeasts [32,36–40]. In addition, the non-polar forces yielding the defined and oriented pCc₁–pCc complex would be determinant in the binding event, as they do in the X-ray structure of the yeast complex III–Cc system [20,30,31]. Thus, the charged residues may provide a first step in recognition via electrostatic steering, which could further result in well-defined and specific orientations governed by hydrophobic contacts at short distances, as proposed for many other electron transient complexes. Actually, the large magnitude of the CSP for the pCc₁–pCc adducts in our solution NMR experiments suggests predominant hydrophobic contacts that extend the time that both heme proteins spend in single orientations. This clearly differs from other Cc-involving interfaces, namely those in the non-physiological complexes Cf–Cc and cytochrome b₅–Cc [73,74].

Our data strongly point that such single orientations of pCc result in two well-defined binding sites on pCc₁: a tight *proximal* site (equilibrium dissociation constant ranging from 0.25 to 9.3 μ M), in which the heme-to-heme distance is optimum for ET and consistent with the

crystallographic structures [20,30,31], and a weak *distal* site (equilibrium dissociation constant ranging from 30 to 110 μ M), in which the heme-to-heme distance is not suitable for ET and is not occupied in the crystal structures. Such a novel *distal* binding site is here evidenced in solution by NMR and ITC experiments with reduced and oxidized pCc and pCc₁, as well as by *ab-initio* BD calculations. In addition, the PCA performed to validate CSP fits reveals a global and majoritarian component that accurately fitted to a 2:1 binding model. Other authors had previously reported the existence of non-ET conformations or evidenced more than one Cc binding site in the Cbc₁–Cc complex [25,26,28,29].

Our NMR-driven docking approach also reveals that such a two-site model is consistent with NMR constraints obtained with the pCc₁–pCc complex at the reduced state. It is worth to mention that pCc uses a common surface area to explore the two binding sites on pCc₁. According to the literature, other c-type cytochromes use the same residues to interact with more than one site at their partner surface, either forming a ternary complex between *Phormidium* Cf and yeast Cc [73] or assembling an encounter complex with *Nostoc* cytochrome c₆ and Cf [75]. The dissociation constants for the two binding sites in the Cf–Cc system are similar to those herein described for the pCc₁–pCc complex, in the μ M range with a highly dynamic behavior. Moreover, the differences in affinity between the two binding sites in the Cf–Cc and Cc₁–Cc complexes are moderate, a finding that is compatible with a linear behavior of the CSPs of Cc amide groups (Fig. 4b) and with a similar chemical environment on the surfaces of Cf and Cc₁, both negatively charged. Indeed, the resulting docking data show that the location of the pCc *distal* binding site into the pCc₁–pCc complex is close to the extended β -strand fingers, in a negative pocket, at physiological ionic strength (Fig. S10) that contact directly with the head of the Rieske subunit.

The docking of pCc at the *distal* binding site is not impeded by the pRieske subunit, and only the relative orientation of pCc₁ and pCc in the transient complex is slightly changed. Similar effects have been observed in BD computations carried out on the photosynthetic ET complex formed by the Cf–Rieske adduct with cytochrome c₆ [77]. In principle, the visualization of the *proximal* but not the *distal* site in X-ray coordinates could be easily explained by assuming a weaker, yet physiological, nature of the *distal* binding site, which would be stable enough to be detected in solution by NMR. Moreover, the binding studies with both redox states indicate that the reduced complex is tighter than the oxidized one, though both systems maintain two pCc binding sites for interaction.

5. Conclusions

Our *in vitro* experiments indicate that the interactions of pCc with the *proximal* and *distal* sites of pCc₁ are two independent binding events. The *distal* site herein reported for the pCc₁–pCc complex opens the possibility to new binding modes in solution for the native dimeric complex III, including the simultaneous allocation of two pCc molecules on the pCc₁ surface without steric hindrance between them (Fig. 7). The extra *distal* site in complex III could indeed be used to facilitate the functional shuttle of electrons to complex IV in plant supercomplexes [18]. Actually, this may provide a path for diffusion of the electron carrier to the oxidase, as the pCc molecules could move from the *distal* to the *proximal* site, and vice versa, so using them as entry or exit ports. In other words, the pCc molecules could serve as a “floating boat bridge” between complexes III and IV within the respirasome rather than as a long distance electron carrier. Also, an extra *distal* site could serve as an attraction for pCc molecules to simply increase its local concentration near binding domains, as was proposed to explain the second Cc₂ binding site in the *Rhodobacter capsulatus* Cbc₁–Cc₂ complex in its oxidized state [29]. The extra *distal* site could have physiological relevance in the dynamics and organization of electron flow, which is modulated in supercomplexes to optimize the use of available substrates [15].

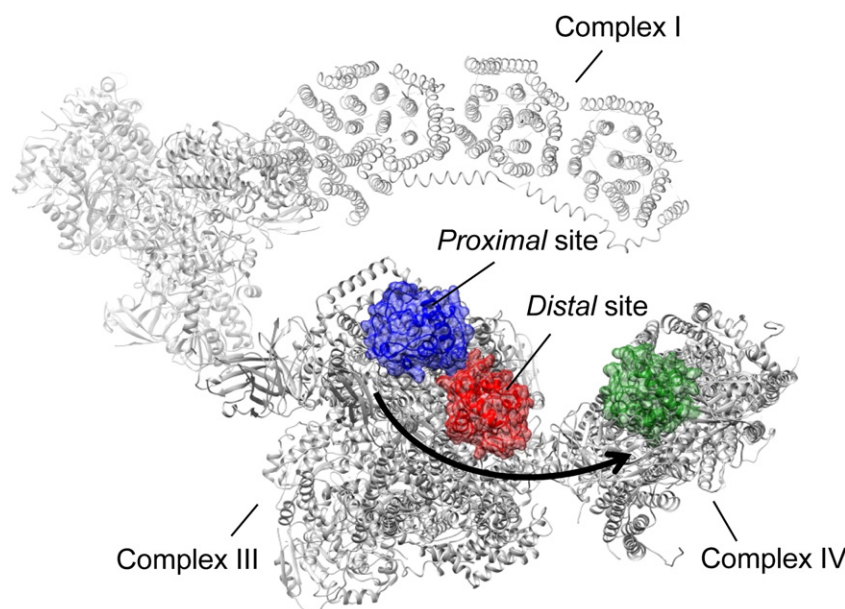


Fig. 7. Binding sites for Cc on complexes III and IV at the respiratory supercomplex. Complexes III and IV (gray) in respiratory supercomplexes are viewed from the mitochondrial inter-membrane space. The representative structure of Cc at the *proximal* site of C_3 is in blue, whereas that at the *distal* site is in red. HADDOCK results were superposed on the monomer of complex III dimer in which Cc binding was reported by X-ray crystallography (PDB ID: 1kvo). Cc was also represented (green) docked to respiratory complex IV, in the proposed binding site for ET to CcO subunit [78]. A putative new way of communication between both complexes through Cc molecules is marked by black arrows. This figure is an adaptation from the fitted model for bovine mitochondrial supercomplex [21].

Acknowledgments

We thank Dr. Manuel Angulo and Dr. Encarnación Zafra for assistance in the NMR data collection at CITIUS NMR Facility at University of Seville. Our special appreciation is addressed to Prof. Menéndez and Dr. Bustamante for the analytical ultracentrifugation experiments performed at the Institute of Physical Chemistry “Rocasolano” (Madrid, Spain). Financial support was provided by the Spanish Ministry of Economy and Competitiveness (Grant Nos. BFU2009-07190/BMC, BFU2010-19451/BMC and BFU2012-31670/BMC) and by the Andalusian Government (Grant PAI, BIO198). BMB was awarded with a PhD fellowship (AP2009-4092) and a short-term travel grant to Prof. Ubbink's laboratory (Leiden University) from the Spanish Ministry of Education, co-funded by European Social Fund-ERDF (2007–2013). All authors declare no conflict of interest.

Appendix A. Supplementary data

Supplementary data to this article can be found online at <http://dx.doi.org/10.1016/j.bbabo.2014.07.017>.

References

- [1] D. Keilin, E.F. Hartree, Relationship between certain components of the cytochrome system, *Nature* 176 (1955) 200–206.
- [2] L. Banci, I. Bertini, K.L. Bren, H.B. Gray, P. Somporpnisut, P. Turano, Solution structure of oxidized *Saccharomyces cerevisiae* Iso-1-cytochrome c, *Biochemistry* 36 (1997) 8992–9001.
- [3] P. Baistrocchi, L. Banci, I. Bertini, P. Turano, K.L. Bren, H.B. Gray, Three-dimensional solution structure of *Saccharomyces cerevisiae* reduced iso-1-cytochrome c, *Biochemistry* 35 (1996) 13788–13796.
- [4] H. Eubel, J. Heinemeyer, S. Sunderhaus, H.P. Braun, Respiratory chain supercomplexes in plant mitochondria, *Plant Physiol. Biochem.* 42 (2004) 937–942.
- [5] N.G. Leferink, W.A. van den Berg, W.J. van Berkel, L-Galactono-gamma-lactone dehydrogenase from *Arabidopsis thaliana*, a flavoprotein involved in vitamin C biosynthesis, *FEBS J.* 275 (2008) 713–726.
- [6] M. Hervás, Q. Bashir, N.G. Leferink, P. Ferreira, B. Moreno-Beltrán, A.H. Westphal, I. Díaz-Moreno, M. Medina, M.A. De la Rosa, M. Ubbink, J.A. Navarro, W.J. van Berkel, Communication between (L)-galactono-1,4-lactone dehydrogenase and cytochrome c, *FEBS J.* 280 (2013) 1830–1840.
- [7] I. Díaz-Moreno, J.M. García-Heredia, A. Díaz-Quintana, M.A. De la Rosa, Cytochrome c signalosome in mitochondria, *Eur. Biophys. J.* 40 (2011) 1301–1315.
- [8] J. Martínez-Fabregas, I. Díaz-Moreno, K. González-Arzola, S. Janocha, J.A. Navarro, M. Hervás, R. Bernhardt, A. Díaz-Quintana, M.A. De la Rosa, New *Arabidopsis thaliana* cytochrome c partners: a look into the elusive role of cytochrome c in programmed cell death in plants, *Mol. Cell. Proteomics* 12 (2013) 3666–3676.
- [9] I. Bertini, S. Chevance, R. Del Conte, D. Lalli, P. Turano, The anti-apoptotic Bcl-x(L) protein, a new piece in the puzzle of cytochrome c interactome, *PLoS ONE* 6 (2011) e18329.
- [10] J. Martínez-Fabregas, I. Díaz-Moreno, K. González-Arzola, S. Janocha, J.A. Navarro, M. Hervás, R. Bernhardt, A. Velazquez-Campoy, A. Díaz-Quintana, M.A. De la Rosa, Structural and functional analysis of novel human cytochrome c targets in apoptosis, *Mol. Cell. Proteomics* 13 (2014) 1439–1456.
- [11] M. Trouillard, B. Meunier, F. Rappaport, Questioning the functional relevance of mitochondrial supercomplexes by time-resolved analysis of the respiratory chain, *Proc. Natl. Acad. Sci. U. S. A.* 108 (2011) 1027–1034.
- [12] C.R. Hackenbrock, B. Chazotte, S.S. Gupte, The random collision model and a critical assessment of diffusion and collision in mitochondrial electron transport, *J. Bioenerg. Biomembr.* 18 (1986) 331–368.
- [13] R. Acín-Pérez, P. Fernández-Silva, M.L. Peleato, A. Pérez-Martos, J.A. Enríquez, Respiratory active mitochondrial supercomplexes, *Mol. Cell* 32 (2008) 529–539.
- [14] G. Lenaz, M.L. Genova, Structure and organization of mitochondrial respiratory complexes: a new understanding of an old subject, *Antioxid. Redox Signal.* 12 (2010) 961–1008.
- [15] E. Lapuente-Brun, R. Moreno-Loshuertos, R. Acín-Pérez, A. Latorre-Pellicer, C. Colás, E. Balsa, E. Perales-Clemente, P.M. Quirós, E. Calvo, M.A. Rodríguez-Hernández, P. Navas, R. Cruz, Á. Carracedo, C. López-Otín, A. Pérez-Martos, P. Fernández-Silva, E. Fernández-Vizarra, J.A. Enríquez, Supercomplex assembly determines electron flux in the mitochondrial electron transport chain, *Science* 340 (2013) 1567–1570.
- [16] H. Eubel, L. Jänsch, H.P. Braun, New insights into the respiratory chain of plant mitochondria. Supercomplexes and a unique composition of complex II, *Plant Physiol.* 133 (2003) 274–286.
- [17] P. Schertl, S. Sunderhaus, J. Klodmann, G.E. Grozeff, C.G. Bartoli, H.P. Braun, L-galactono-1,4-lactone dehydrogenase (GLDH) forms part of three subcomplexes of mitochondrial complex I in *Arabidopsis thaliana*, *J. Biol. Chem.* 287 (2012) 14412–14419.
- [18] M.L. Genova, G. Lenaz, A critical appraisal of the role of respiratory supercomplexes in mitochondria, *Biol. Chem.* 394 (2013) 631–639.
- [19] B.N. Kholodenko, H.V. Westerhoff, Metabolic channelling and control of the flux, *FEBS Lett.* 320 (1993) 71–74.
- [20] S.R. Solmaz, C. Hunte, Structure of complex III with bound cytochrome c in reduced state and definition of a minimal core interface for electron transfer, *J. Biol. Chem.* 283 (2008) 17542–17549.
- [21] T. Althoff, D.J. Mills, J.L. Popot, W. Kühlbrandt, Arrangement of electron transport chain components in bovine mitochondrial supercomplex I₁III₂IV₁, *EMBO J.* 30 (2011) 4652–4664.

- [22] J.B. Bultema, H.P. Braun, E.J. Boekema, R. Kouril, Megacomplex organization of the oxidative phosphorylation system by structural analysis of respiratory supercomplexes from potato, *Biochim. Biophys. Acta* 1787 (2009) 60–67.
- [23] O. Maneg, F. Malatesta, B. Ludwig, V. Drosou, Interaction of cytochrome *c* with cytochrome oxidase: two different docking scenarios, *Biochim. Biophys. Acta* 1655 (2004) 274–281.
- [24] J. Janzon, Q. Yuan, F. Malatesta, P. Hellwig, B. Ludwig, B. Durham, F. Millet, Probing the *Paracoccus denitrificans* cytochrome *c*₁/cytochrome *c*₅₅₂ interaction by mutagenesis and fast kinetics, *Biochemistry* 47 (2008) 12974–12984.
- [25] S.H. Speck, D. Dye, E. Margoliash, Single catalytic site model for the oxidation of ferrocycytochrome *c* by mitochondrial cytochrome *c* oxidase, *Proc. Natl. Acad. Sci. U. S. A.* 81 (1984) 347–351.
- [26] E.A. Garber, E. Margoliash, Interaction of cytochrome *c* with cytochrome *c* oxidase: an understanding of the high- to low-affinity transition, *Biochim. Biophys. Acta* 1015 (1990) 279–287.
- [27] K. Sakamoto, M. Kamiya, M. Imai, K. Shinzawa-Itoh, T. Uchida, K. Kawano, S. Yoshikawa, K. Ishimori, NMR basis for interprotein electron transfer gating between cytochrome *c* and cytochrome *c* oxidase, *Proc. Natl. Acad. Sci. U. S. A.* 108 (2011) 12271–12276.
- [28] S.H. Speck, E. Margoliash, Characterization of the interaction of cytochrome *c* and mitochondrial ubiquinol-cytochrome *c* reductase, *J. Biol. Chem.* 259 (1984) 1064–1072.
- [29] S. Devanathan, Z. Salamon, G. Tollin, J.C. Fitch, T.E. Meyer, E.A. Berry, M.A. Cusanovich, Plasmon waveguide resonance spectroscopic evidence for differential binding of oxidized and reduced *Rhodobacter capsulatus* cytochrome *c*₂ to the cytochrome *bc*₁ complex mediated by the conformation of the Rieske iron-sulfur protein, *Biochemistry* 46 (2007) 7138–7145.
- [30] C. Lange, C. Hunte, Crystal structure of the yeast cytochrome *bc*₁ complex with its bound substrate cytochrome *c*, *Proc. Natl. Acad. Sci. U. S. A.* 99 (2002) 2800–2805.
- [31] A. Nyola, C. Hunte, A structural analysis of the transient interaction between the cytochrome *bc*₁ complex and its substrate cytochrome *c*, *Biochem. Soc. Trans.* 36 (2008) 981–985.
- [32] O. Kokhan, C.A. Wraight, E. Tajkhorshid, The binding interface of cytochrome *c* and cytochrome *c*₁ in the *bc*₁ complex: rationalizing the role of key residues, *Biophys. J.* 99 (2010) 2647–2656.
- [33] S.H. Speck, S. Ferguson-Miller, N. Osheroff, E. Margoliash, Definition of cytochrome *c* binding domains by chemical modification: kinetics of reaction with beef mitochondrial reductase and functional organization of the respiratory chain, *Proc. Natl. Acad. Sci. U. S. A.* 76 (1979) 155–159.
- [34] B.W. König, N. Osheroff, J. Wilms, A.O. Muijsers, H.L. Dekker, E. Margoliash, Mapping of the interaction domain for purified cytochrome *c*₁ on cytochrome *c*, *FEBS Lett.* 111 (1980) 395–398.
- [35] M. Sarewicz, A. Borek, F. Daldal, W. Froncisz, A. Osyczka, Demonstration of short-lived complexes of cytochrome *c* with cytochrome *bc*₁ by EPR spectroscopy: implications for the mechanism of interprotein electron transfer, *J. Biol. Chem.* 283 (2008) 24826–24836.
- [36] F. Millett, J. Havens, S. Rajagukguk, B. Durham, Design and use of photoactive ruthenium complexes to study electron transfer within cytochrome *bc*₁ and from cytochrome *bc*₁ to cytochrome *c*, *Biochim. Biophys. Acta* 1827 (2013) 1309–1319.
- [37] G. Engstrom, R. Rajagukguk, A.J. Saunders, C. Patel, S. Rajagukguk, T. Merbitz-Zahradnik, K. Xiao, G. Pielak, B. Trumpower, C. Yu, L. Yu, B. Durham, F. Millett, Design of a ruthenium-labeled cytochrome *c* derivative to study electron transfer with the cytochrome *bc*₁ complex, *Biochemistry* 42 (2003) 2816–2824.
- [38] H. Tian, R. Sadoski, L. Zhang, C. Yu, L. Yu, B. Durham, F. Millett, Definition of the interaction domain of the cytochrome *c* on the cytochrome *bc*₁ complex. Steady-state and rapid kinetic analysis of electron transfer between cytochrome *c* and *Rhodobacter sphaeroides* cytochrome *bc*₁ surface mutants, *J. Biol. Chem.* 275 (2000) 9587–9595.
- [39] F. Millett, B. Durham, Kinetics of Electron transfer within cytochrome *bc*₁ and Between cytochrome *bc*₁ and cytochrome *c*, *Photosynth. Res.* 82 (2004) 1–16.
- [40] M. Castellani, J. Havens, T. Kleinschroth, F. Millett, B. Durham, F. Malatesta, B. Ludwig, The acidic domain of cytochrome *c*₁ in *Paracoccus denitrificans*, analogous to the acidic subunits in eukaryotic *bc*₁ complexes, is not involved in the electron transfer reaction to its native substrate cytochrome *c*₅₅₂, *Biochim. Biophys. Acta* 1807 (2011) 1383–1389.
- [41] A. Olteanu, C.N. Patel, M.M. Dedmon, S. Kennedy, M.W. Linhoff, C.M. Minder, P. R. Potts, M. Deshmukh, G.J. Pielak, Stability and apoptotic activity of recombinant human cytochrome *c*, *Biochem. Biophys. Res. Commun.* 312 (2003) 733–740.
- [42] V. Rodríguez-Roldán, J.M. García-Heredia, J.A. Navarro, M. Hervás, B. De la Cerda, F.P. Molina-Heredia, M.A. De la Rosa, A comparative kinetic analysis of the reactivity of plant, horse, and human respiratory cytochrome *c* towards cytochrome *c* oxidase, *Biochem. Biophys. Res. Commun.* 346 (2006) 1108–1113.
- [43] N. Sreerama, R.W. Woody, Estimation of protein secondary structure from circular dichroism spectra: comparison of CONTIN, SELCON, and CDSSTR methods with an expanded reference set, *Anal. Biochem.* 287 (2000) 252–260.
- [44] N. Sreerama, R.W. Woody, Computation and analysis of protein circular dichroism spectra, *Methods Enzymol.* 383 (2004) 318–351.
- [45] P. Schuck, Size-distribution analysis of macromolecules by sedimentation velocity ultracentrifugation and lamm equation modeling, *Biophys. J.* 78 (2000) 1606–1619.
- [46] T.M. Laue, B.D. Shah, T.M. Ridgeway, S.L. Pelletier, Computer-aided interpretation of analytical sedimentation data for proteins, in: S. Harding, A. Rowe, J. Horton (Eds.), *Analytical Ultracentrifugation in Biochemistry and Polymer Science*, Royal Society of Chemistry, Cambridge, 1992, pp. 90–125, (United Kingdom).
- [47] M. Piotto, V. Saudek, V. Sklenár, Gradient-tailored excitation for single-quantum NMR spectroscopy of aqueous solutions, *J. Biomol. NMR* 2 (1992) 661–665.
- [48] Z.X. Wang, R.F. Jiang, A novel two-site binding equation presented in terms of the total ligand concentration, *FEBS Lett.* 392 (1996) 245–249.
- [49] E. Freire, A. Schön, A. Velázquez-Campoy, Isothermal titration calorimetry: general formalism using binding polynomials, *Methods Enzymol.* 455 (2009) 127–155.
- [50] R.R. Gabdouliline, R.C. Wade, Brownian dynamics simulation of protein-protein diffusional encounter, *Methods* 14 (1998) 329–341.
- [51] J. Wang, W. Wang, P.A. Kollman, D.A. Case, Automatic atom type and bond type perception in molecular mechanical calculations, *J. Mol. Graph. Model.* 25 (2006) 247–260.
- [52] Y. Duan, C. Wu, S. Chowdhury, M.C. Lee, G. Xiong, W. Zhang, R. Yang, P. Cieplak, R. Luo, T. Lee, J. Caldwell, J. Wang, P. Kollman, A point-charge force field for molecular mechanics simulations of proteins based on condensed-phase quantum mechanical calculations, *J. Comput. Chem.* 24 (2003) 1999–2012.
- [53] N.A. Baker, D. Sept, S. Joseph, M.J. Holst, J.A. McCammon, Electrostatics of nanosystems: application to microtubules and the ribosome, *Proc. Natl. Acad. Sci. U. S. A.* 98 (2001) 10037–10041.
- [54] I. Díaz-Moreno, F.J. Muñoz-López, E. Frutos-Beltrán, M.A. De la Rosa, A. Díaz-Quintana, Electrostatic strain and concerted motions in the transient complex between plastocyanin and cytochrome *f* from the cyanobacterium *Phormidium laminosum*, *Bioelectrochemistry* 77 (2009) 43–52.
- [55] W. Humphrey, A. Dalke, K. Schulten, VMD: visual molecular dynamics, *J. Mol. Graph.* 14 (1996) 33–38.
- [56] E.F. Pettersen, T.D. Goddard, C.C. Huang, G.S. Couch, D.M. Greenblatt, E.C. Meng, T.E. Ferrin, UCSF Chimera—A visualization system for exploratory research and analysis, *J. Comput. Chem.* 25 (2004) 1605–1612.
- [57] C. Dominguez, R. Boelens, A.M. Bonvin, HADDOCK: a protein–protein docking approach based on biochemical or biophysical information, *J. Am. Chem. Soc.* 125 (2003) 1731–1737.
- [58] A.D. van Dijk, R. Boelens, A.M. Bonvin, Data-driven docking for the study of biomolecular complexes, *FEBS J.* 272 (2005) 293–312.
- [59] S.J. de Vries, A.D. van Dijk, M. Krzeminski, M. van Dijk, A. Thureau, V. Hsu, T. Wassenaar, A.M. Bonvin, HADDOCK versus HADDOCK: new features and performance of HADDOCK2.0 on the CAPRI targets, *Proteins* 69 (2007) 726–733.
- [60] Z. Zhang, L. Huang, V.M. Shulmeister, Y.I. Chi, K.K. Kim, L.W. Hung, A.R. Crofts, E.A. Berry, S.H. Kim, Electron transfer by domain movement in cytochrome *bc*₁, *Nature* 392 (1998) 677–684.
- [61] Y. Li, K. Leonard, H. Weiss, Membrane-bound and water-soluble cytochrome *c*₁ from *Neurospora mitochondria*, *Eur. J. Biochem.* 116 (1981) 199–205.
- [62] K. Konishi, S.R. Van Doren, D.M. Kramer, A.R. Crofts, R.B. Gennis, Preparation and characterization of the water-soluble heme-binding domain of cytochrome *c*₁ from the *Rhodobacter sphaeroides* *bc*₁ complex, *J. Biol. Chem.* 266 (1991) 14270–14276.
- [63] T. Meyer, J. Gross, C. Blanck, M. Schmutz, B. Ludwig, P. Hellwig, F. Melin, Electrochemistry of cytochrome *c*₁, cytochrome *c*₅₅₂, and Cu_A from the respiratory chain of *Thermus thermophilus* immobilized on gold nanoparticles, *J. Phys. Chem. B* 115 (2011) 7165–7170.
- [64] C. Albarrán, J.A. Navarro, F.P. Molina-Heredia, P.S. Murdoch, M.A. De la Rosa, M. Hervás, Laser flash-induced kinetic analysis of cytochrome *f* oxidation by wild-type and mutant plastocyanin from the cyanobacterium *Nostoc sp. PCC 7119*, *Biochemistry* 44 (2005) 11601–11607.
- [65] I. Díaz-Moreno, A. Díaz-Quintana, M.A. De la Rosa, M. Ubbink, Structure of the complex between plastocyanin and cytochrome *f* from the cyanobacterium *Nostoc sp. PCC 7119* as determined by paramagnetic NMR. The balance between electrostatic and hydrophobic interactions within the transient complex determines the relative orientation of the two proteins, *J. Biol. Chem.* 280 (2005) 18908–18915.
- [66] E.A. Berry, L.S. Huang, V.J. DeRose, Ubiquinol-cytochrome *c* oxidoreductase of higher plants. Isolation and characterization of the *bc*₁ complex from potato tuber mitochondria, *J. Biol. Chem.* 266 (1991) 9064–9077.
- [67] K.M. Andrews, A.R. Crofts, R.B. Gennis, Large-scale purification and characterization of a highly active four-subunit cytochrome *bc*₁ complex from *Rhodobacter sphaeroides*, *Biochemistry* 29 (1990) 2645–2651.
- [68] A.Y. Mulikidjanian, Ubiquinol oxidation in the cytochrome *bc*₁ complex: reaction mechanism and prevention of short-circuiting, *Biochim. Biophys. Acta* 1709 (2005) 5–34.
- [69] M. Ubbink, M. Ejdeback, B.G. Karlsson, D.S. Bendall, The structure of the complex of plastocyanin and cytochrome *f*, determined by paramagnetic NMR and restrained rigid-body molecular dynamics, *Structure* 6 (1998) 323–335.
- [70] I. Díaz-Moreno, A. Díaz-Quintana, F.P. Molina-Heredia, P.M. Nieto, O. Hansson, M.A. De la Rosa, B.G. Karlsson, NMR analysis of the transient complex between membrane photosystem I and soluble cytochrome *c*₆, *J. Biol. Chem.* 280 (2005) 7925–7931.
- [71] I. Díaz-Moreno, A. Díaz-Quintana, M. Ubbink, M.A. De la Rosa, An NMR-based docking model for the physiological transient complex between cytochrome *f* and cytochrome *c*₆, *FEBS Lett.* 579 (2005) 2891–2896.
- [72] J.A. Worrall, U. Kolczak, G.W. Canters, M. Ubbink, Interaction of yeast iso-1-cytochrome *c* with cytochrome *c* peroxidase investigated by [¹⁵N, ¹H] heteronuclear NMR spectroscopy, *Biochemistry* 40 (2001) 7069–7076.
- [73] P.B. Crowley, K.S. Rabe, J.A. Worrall, G.W. Canters, M. Ubbink, The ternary complex of cytochrome *f* and cytochrome *c*: identification of a second binding site and competition for plastocyanin binding, *Chembiochem* 3 (2002) 526–533.

- [74] A.N. Volkov, D. Ferrari, J.A. Worrall, A.M. Bonvin, M. Ubbink, The orientations of cytochrome *c* in the highly dynamic complex with cytochrome *b*₅ visualized by NMR and docking using HADDOCK, *Protein Sci.* 14 (2005) 799–811.
- [75] I. Díaz-Moreno, R. Hulsker, P. Skubak, J.M. Foerster, D. Cavazzini, M.G. Finiguerra, A. Díaz-Quintana, B. Moreno-Beltrán, G.L. Rossi, G.M. Ullmann, N.S. Pannu, M.A. De la Rosa, M. Ubbink, The dynamic complex of cytochrome *c*₆ and cytochrome *f* studied with paramagnetic NMR spectroscopy, *Biochim. Biophys. Acta* 1837 (2014) 1305–1315.
- [76] J.C. Ferreón, C.W. Lee, M. Arai, M.A. Martínez-Yamout, H.J. Dyson, P.E. Wright, Cooperative regulation of p53 by modulation of ternary complex formation with CBP/p300 and HDM2, *Proc. Natl. Acad. Sci. U. S. A.* 106 (2008) 6591–6596.
- [77] E.J. Haddadian, E.L. Gross, A Brownian dynamics study of the interactions of the luminal domains of the cytochrome *b*₆*f* complex with plastocyanin and cytochrome *c*₆: the effects of the Rieske FeS protein on the interactions, *Biophys. J.* 91 (2006) 2589–2600.
- [78] D. Flöck, V. Helms, Protein-protein docking of electron transfer complexes: cytochrome *c* oxidase and cytochrome *c*, *Proteins* 47 (2002) 75–85.